Journal of Molecular Structure 993 (2011) 2–8

Contents lists available at ScienceDirect

Journal of Molecular Structure

journal homepage: www.elsevier.com/locate/molstruc

Rotationally resolved electronic spectroscopy of 2,3-bridged indole derivatives: Tetrahydrocarbazole

Olivia Oeltermann [a], Christian Brand [a], W. Leo Meerts [b], Jörg Tatchen [c], Michael Schmitt [a,*]

[a] Heinrich-Heine-Universität, Institut für Physikalische Chemie I, Universitätsstrasse 26.43, D-40225 Düsseldorf, Germany
[b] Radboud University, Institute for Molecules and Materials, Heyendaalseweg 135, NL-6525 AJ Nijmegen, The Netherlands
[c] Heinrich-Heine-Universität, Institut für Theoretische Chemie und Computerchemie, Universitätsstrasse 26.32, D-40225 Düsseldorf, Germany

ARTICLE INFO

Article history:
Available online 25 February 2011

Keywords:
Electronic spectroscopy
Rotationally resolved spectroscopy
Structural analysis
Ab initio theory
Excited states
Evolutionary algorithms

ABSTRACT

The rotationally resolved electronic spectrum of tetrahydrocarbazole seeded in a molecular beam has been taken. The lowest excited singlet state of tetrahydrocarbazole could be shown to have L_a character, in contrast to nearly all other indole derivatives, which have the L_b as lowest state. An upper limit for the energy difference of both states can be estimated to be 1000 cm^1 with the L_b state being structurally and energetically close to the intersection of both states. Comparison of the rotational constants and the vibrational wavenumbers to the results of *ab initio* calculations shows, that the saturated six-ring is in a twisted configuration in both electronic states.

1. Introduction

The energy ordering of the lowest electronically excited singlet states of indole and indole derivatives has found considerable interest in the last few decades owing to the large sensitivity of the fluorescence properties of the indole chromophore on the environment [1–19]. Tetrahydrocarbazole (THC), shown in Fig. 1 is the bridged analog of the indole derivative 2,3-dimethylindole, which is known to have a very small energy gap between the lowest two excited singlet states. These are labeled L_a and L_b in the nomenclature of Platt [20].

A very small L_a/L_b energy gap is also expected for THC. For 2,3-dimethylindole the energetic ordering of the ^1L_a and ^1L_b states is subject of a long-lasting debate. Two-photon intensity ratios for linear versus circular polarized excitation, taken by Short and Callis [21], showed that the origin band of the isolated molecule in the gas-phase has L_b character, and the first band with L_a character appears 342 cm^1 above the origin. The extreme dependence of the relative positions of L_a and L_b states in 2,3-dimethylindole on the local surrounding is illustrated by the fact, that even in a very non-polar media, the energetic order of L_a and L_b states is interchanged, as determined by Fender and Callis via fluorescence anisotropy of 2,3-dimethylindole in an argon matrix, [22] and by Rehms and Callis [23] in cyclohexane solution, where the ^1L_a state is found to be below the ^1L_b state. This dependence of the energetic ordering of L_a andL_b states in 2,3-dimethylindole on the local surrounding sets the stage for the present investigation. If the small difference in going from non-polar solvent to vacuum is sufficient to reverse the state order, the question arises if bridging the 2,3 position as in THC introduces a perturbation large enough to draw the ^1L_a below the ^{1} L_b origin, already for the isolated molecule. Teh et al. presented fluorescence lifetime values, which are consistent with the L_a state lying below L_b but give no definite evidence [24].

The change in bond length between the carbon atoms 2 and 3 of the pyrrole ring (see Fig. 1) constitutes a coordinate, which has been postulated to be the tuning mode for the L_b/L_a conical intersection in indole by Callis [25]. If this is true, the question arises, what will happen to the energy ordering and intersection of these two states, once the tuning coordinate is manipulated. The tuning coordinate is an intramolecular coordinate, along which the energy difference of the two states connected by a conical intersection is modulated. The formation of a six-ring by bridging the 2 and 3 position of indole with a $-(CH_2)_4-$ chain opens the possibility for different ring conformations. Planar, boat, chair and twist conformations are possible and can be distinguished by their rotational constants and different inertial defects. Aminosubstituted tetrahydrocarbazoles are utilized as conformationally restricted neurotransmitter analogs with high specificity for the 5-$HT_{1D\beta}$ receptor.

Hager et al. presented the electronic spectra of jet-cooled tetrahydrocarbazole [26]. They reported fluorescence life times of 3.9 ns at the vibrationless origin at 34793 cm^1 and a considerable shortening to 1.1 ns already at 400 cm^1 excess energy. These life times are much shorter than those of the parent molecule indole itself. Dispersed fluorescence spectra of selected vibrational bands of

* Corresponding author.
E-mail address: mschmitt@uni-duesseldorf.de (M. Schmitt).

0022-2860/$ - see front matter © 2011 Elsevier B.V. All rights reserved.
doi:10.1016/j.molstruc.2011.01.029

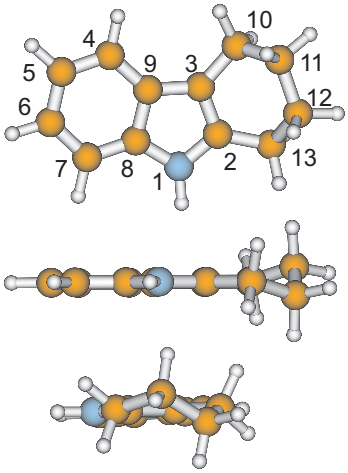

Fig. 1. Three different views of the structure of the twist conformer of THC in its electronic ground state along with the atomic numbering used.

tetrahydrocarbazole were presented by Demmer et al. [27]. They also measured the fluorescence life times of vibronic bands of N-deuterated tetrahydrocarbazole with marked longer life times (>10 ns) than for the undeuterated compound.

In the present paper we investigate the structures of THC in its ground and electronically excited states from rotationally resolved electronic spectroscopy.

2. Techniques

2.1. Experimental procedures

THC ($\geqslant$99%) was purchased from Fluka and used without further purification. The experimental setup is described in detail elsewhere [28]. In brief, the laser system consists of a single frequency ring dye laser (Sirah Matisse DS) operated with Rhodamine 6G, pumped with 6 W of the 532 nm line of a frequency doubled CW Nd:YAG laser (Spectra Physics Millenium X). The dye laser output was coupled into an external folded ring cavity (Spectra Physics Wavetrain) for second harmonic generation. The resulting output power was about 25 mW. The molecular beam was formed by co-expanding tetrahydrocarbazole, heated to 160 °C, and 600 mbar of argon through a 200 µm nozzle into the vacuum chamber. The molecular beam machine consists of three differentially pumped vacuum chambers that are linearly connected by skimmers (1 mm and 3 mm, respectively) in order to reduce the Doppler width. The resulting resolution is 15 MHz (FWHM) in this setup. In the third chamber, 360 mm downstream of the nozzle, the molecular beam crosses the laser beam at a right angle. The imaging optics setup consists of a concave mirror and two plano-convex lenses to focus the resulting fluorescence onto a photomultiplier tube, which is mounted perpendicularly to the plane defined by the laser and molecular beam. The signal output was then discriminated and digitized by a photon counter and transmitted to a PC for data recording and processing. The relative frequency was determined with a *quasi* confocal Fabry–Perot interferometer. The absolute frequency was obtained by comparing the recorded spectrum to the tabulated lines in the iodine absorption spectrum [29].

2.2. Computational methods

2.2.1. Quantum chemical calculations

Structure optimizations were performed employing the correlation consistent Polarized Valence Triple Zeta (cc-pVTZ) basis from the TURBOMOLE library [30,31]. The equilibrium geometries of the electronic ground and the lowest excited singlet states were optimized using the approximate coupled cluster singles and doubles model (CC2) employing the resolution-of-the-identity approximation (RI) [32–34].

At the optimized geometries, additional single-point electronic spectra were calculated using the combined density functional theory/multi-reference configuration interaction (DFT/MRCI) method developed by Grimme and Waletzke [35]. Configuration state functions (CSFs) in the MRCI expansion were constructed from Kohn–Sham (KS) orbitals, optimized for the dominant closed shell determinant of the electronic ground state employing the BH-LYP [36,37] functional. All 56 valence electrons were correlated in the MRCI runs and the eigenvalues and eigenvectors of five singlet states were determined. The *initial* set of reference configuration state functions was generated automatically in a complete active space type procedure (including all single and double excitations from the five highest occupied molecular orbitals in the KS determinant to the five lowest virtual orbitals). The set was then iteratively improved. The MRCI expansion was kept moderate by extensive configuration selection. The selection of the most important CSFs is based on an energy gap criterion as described in Ref. [35]. Only those configurations were taken into account that have an energy below a certain cutoff energy. The energy of a given configuration was estimated from orbital energies within the selection procedure. The cutoff energy was given by the energy of the highest desired root as calculated for the reference space plus a cutoff parameter $\delta E_{sel} = 1.0E_H$. The latter choice has been shown to yield nearly converged results [35].

2.2.2. Fits of the rovibronic spectra using evolutionary algorithms

The rovibronic spectra were fit using the Covariance Matrix Adaptation Evolution Strategy (CMA-ES), which is an evolutionary algorithm for difficult non-linear non-convex optimization problems in continuous representation. It turns out to be a particularly reliable and highly competitive evolutionary algorithm for local and global optimization. [38] Trial solutions are computed and evaluated according to their correlation with the experimental spectrum. Based on this result, the following generation is constructed. In evolutionary strategies, new generations are created as a random distribution around a single point in the search space. For the CMA-ES, this point is computed from a weighted sum of selected individuals from the foregoing generation using the covariance matrix. The covariance matrix is expected to shape the distribution of the generated individuals in such a way that it adapts to the multidimensional function space. If the correlation is positive, the solution is expected to be further away, and the path step-size is increased. If the step-size is too large, on the other hand, the following generations tend to cancel each other out. This leads to a negative covariance and the step-size is decreased. For a detailed description of the fitting strategy cf. Ref. [39].

3. Results and discussion

3.1. Quantum chemical calculations

Structure optimizations of THC in its electronic ground state were performed with three different starting structures, using the approximate coupled cluster singles and doubles model CC2 within the resolution-of-the-identity approximation (RI) with the triple-ζ cc-pVTZ basis set. The starting structures can be described by the conformations of the saturated six-ring as twist, chair, boat and planar. Actually, the latter form is C_s-symmetric, but not planar, since the aliphatic H-atoms are out-of-plane. Nevertheless we will speak in the following of a planar structure for the sake of simplicity. No stable boat and chair minima were found, instead all optimizations with these starting structures ended in the twist

conformer minimum. The calculated rotational constants of twist and planar THC are compiled in Table 1. They will be compared to the results of the experiment in Section 3.2. As a preliminary result of this comparison, we will use here the fact, that the structure of THC is twist and we will consequently extend our calculations on excited states only on the twist form.

The CC2 optimized structural parameters of the electronically excited singlet states of the twist conformer of THC are compiled in Table 1. They are given as changes, relative to the ground state parameters in the second column of this table. Since the electronic origin in the low resolution excitation spectrum of THC is by far the most intense transition, we exclude the possibility, that the excited state structure is different from the twist form. The lowest excited singlet state has an adiabatic excitation energy (DFT/MRCI zero-point energy corrected) of 34,976 cm^1. It is a nearly pure HOMO → LUMO transition and can be classified in Platt's scheme as being of L_a character. Its transition dipole moment (TDM) makes an angle of 47° with the inertial *a*-axis. The geometry changes upon excitation in the chromophore moiety are very similar to those calculated for the L_a state of indole itself [18].

No stable minimum exhibiting L_b character with respect to the electronic structure could be found on the adiabatic S_1 potential energy surface. Vertical excitation in the Franck–Condon region leads to a state which is composed of HOMO − 1 → LUMO and HOMO → LUMO + 2 and can therefore be classified as L_b state. Relaxation from this geometry as starting point always ended up in the L_a state minimum. Careful inspection of the excitation scheme of each optimization step showed, that in the beginning, the total energy decreased rapidly, and the excited state remained of L_b character. Around 1000 cm^1 above the L_a minimum, the excitation started to change its orbital character and developed into a pure L_a state. Also around this energy, the gradients of the energy became very small, so that we assume a very shallow minimum of the L_b state to exist in this region. A reduction of the step-size of the coordinate update in the optimization also did not lead to a stable minimum. The values for the structure we quote in Table 1 are taken at this point, and serve merely for comparison to the indole system, where the L_b state is the lowest excited singlet state. The comparison of the geometry changes in the L_b state of THC to those of the indole chromophore show, that the assignment of the turning point of the potential energy to the L_b state is reasonable.

Table 1
CC2/cc-pVTZ calculated rotational constants and structural parameters of the twist form of THC in its electronic ground and lowest excited singlet states. Distances (*r*) and their changes upon excitation are given in pm, angles (*a*) and dihedral angles (*d*) in degrees; the full structures are given in the online supplementary material. For the numbering scheme refer to Fig. 1. The calculated geometry changes (CC2/cc-pVTZ) in indole have been taken from Ref. [18] and are given for comparison.

		THC		Indole	
	S_0	$S_1(L_a)$	$S_2(L_b)$	L_a[18]	L_b[18]
A (MHz)	2050	2026	2038		
B (MHz)	563	560	553		
C (MHz)	450	447	443		
r(N1–C2)	138.2	−4.8	+3.2	−3.6	+4.0
r(C2–C3)	137.9	+6.9	+1.4	+6.3	+0.6
r(C3–C9)	143.0	−0.5	+0.5	−0.9	−0.2
r(C4–C5)	139.0	+3.7	+4.2	+3.9	+4.6
r(C5–C6)	140.8	−2.1	+0.4	−2.8	+1.5
r(C6–C7)	139.1	+4.9	+4.5	+6.6	+3.9
r(C7–C8)	139.6	+0.9	+0.1	−0.6	+1.2
r(C8–C9)	142.5	−2.1	+2.7	−1.2	+4.0
r(N1–C8)	137.8	+4.8	−0.7	+3.6	−1.6
r(N1–H1)	100.6	+0.7	+0.6	+0.5	+0.3
r(C4–C9)	140.4	+2.3	+0.7	+1.9	+0.6
r(C3–C10)	149.4	−1.4	−0.5		
r(C10–C11)	153.1	+0.1	+0.0		
r(C11–C12)	152.9	+0.0	+0.1		
r(C12–C13)	153.2	+0.2	+1.3		
r(C13–C2)	148.9	−0.8	−1.0		
a(C3–C10–C11)	109.6	+1.4	+0.1		
a(C10–C11–C12)	111.3	+0.2	−1.6		
a(C11–C12–C13)	111.1	−0.3	+0.3		
a(C12–C13–C2)	108.4	−0.1	+0.9		
a(C13–C2–C3)	126.0	−0.8	+1.5		
a(C2–C3–C10)	122.6	−1.8	−1.2		
d(C4–C9–C3–C10)	−0.3	+0.4	−3.1		
d(C9–C3–C10–C11)	−164.2	−0.1	+3.4		
d(C3–C10–C11–C12)	−47.1	−0.2	−0.7		
d(C10–C11–C12–C13)	+65.8	+0.3	−0.1		
d(C11–C012–C13–C2)	−46.4	−3.6	−0.2		
d(C12–C13–C2–C3)	−15.1	−7.3	−2.5		
d(C13–C2–C3–C10)	+0.3	−7.4	−3.8		

Table 2 presents the vibrational frequencies calculated for the twist form of THC in its ground and electronically excited L_a state at the CC2/cc-pVTZ level of theory and compares them to experimentally determined ones from the PhD thesis of Feng [40]. A very good agreement of the calculated to the measured vibrational wavenumbers for both ground and excited states is obtained. The last column of Table 2 gives the largest coefficients of the Dushinsky matrix, which represent the projections of the excited state vibrational modes on the ground state modes.

The complete 72 × 72 Dushinsky matrix is shown graphically in Fig. 2 and compared to the Dushinsky matrix of the indole chromophore. The Dushinsky matrix has been calculated using the numerically determined Hessian[1] at the CC2/cc-pVTZ optimized structures. The values of the matrix elements are gray coded from white (zero) to black (one). Most of the excited state modes project directly on the ground state modes and are therefore located on the diagonal of the matrix. Deviations are mostly due to deformation vibrations of the saturated six-ring, while the indole centered vibrations mix only weakly.

3.2. Rotationally resolved electronic spectrum of the origin band of THC

Fig. 3 shows the experimental spectrum of the electronic origin of THC. The spectrum was fit with an asymmetric rotor Hamiltonian including axis reorientation [41] using a Covariance Matrix Adaptation (CMA) evolutionary strategy (ES) [38]. For the calculation of the rovibronic intensities, the rotational wave functions of the ground and the excited state have to be expressed in a common coordinate system. This can be achieved for molecules with the transition dipole moment in the molecular plane and the *c*-axis perpendicular to this plane by transforming the excited state rotational Hamiltonian *via* a rotation around the *c*-axis by an angle θ_T[42], which is called the axis reorientation angle.

The axis reorientation angle θ_T has been determined from the CC2/cc-pVTZ *ab initio* structures, using the relation for planar molecules given by Hougen and Watson [41]:

$$tan(\theta_T) = \frac{\sum_i m_i (a_i' b_i'' - b_i' a_i'')}{\sum_i m_i (a_i' a_i'' + b_i' b_i'')} \quad (1)$$

where the doubly primed coordinates refer to the principal axis system in the electronic ground state and the singly primed quantities to the respective excited state inertial system and the mi are the atomic masses. From the CC2/cc-pVTZ optimized structures for the twist and planar forms of THC, we obtained a reorientation angle of −0.67° for the excitation to the L_a state of the twist form and of −0.05° for the planar form. Both the twist and C_s-symmetric forms are slightly non-planar. For the out-of-plane atoms, we used the projections into the indole plane.

[1] Numerical second derivatives obtained using the NumForce script of the Turbomole program package [30].

Table 2
Calculated and experimental vibrational wavenumbers (cm^{-1}) of THC in its S_0 and S_1 electronic states along with the coefficients of the Dushinsky matrix.

Nr.	Calc. (S_0)	Exp. [40]	Calc. (S_1)	Exp. [40]	Dushinsky
1	92.03		81.80	108	$\nu_1(S_1) = +0.97\nu_1(S_0)$
2	139.16	133	107.27		$\nu_2(S_1) = +0.91\nu_2(S_0)$
3	186.56		130.75	140	$\nu_3(S_1) = +0.68\nu_3(S_0) - 0.37\nu_5(S_0)$
4	198.67	200	192.41	190	$\nu_4(S_1) = +0.99\nu_4(S_0)$
5	260.68	266	203.27	195	$\nu_5(S_1) = +0.54\nu_6(S_0) + 0.36\nu_5(S_0)$
6	303.31		266.64	260	$\nu_6(S_1) = +0.65\nu_{10}(S_0) - 0.41\nu_{20}(S_0)$
7	323.69		295.19	284	$\nu_7(S_1) = +0.66\nu_5(S_0) + 0.58\nu_7(S_0)$
8	372.10		319.66	302	$\nu_8(S_1) = -0.62\nu_7(S_0) + 0.49\nu_6(S_0)$
9	386.77		337.01	334	$\nu_9(S_1) = +0.58\nu_{21}(S_0) + 0.49\nu_{10}(S_0)$
10	429.32	428	375.00	387	$\nu_{10}(S_1) = -0.97\nu_9(S_0)$
11	460.23		411.39		$\nu_{11}(S_1) = +0.49\nu_{25}(S_0) + 0.46\nu_{10}(S_0)$
12	495.30	500	450.40		$\nu_{12}(S_1) = -0.99\nu_{11}(S_0)$
13	542.62	547	480.47	489	$\nu_{13}(S_1) = -0.87\nu_{12}(S_0) - 0.45\nu_{13}(S_0)$
14	574.11		498.15		$\nu_{14}(S_1) = -0.87\nu_{14}(S_0)$
15	595.50	601	503.30	512	$\nu_{15}(S_1) = +0.82\nu_{13}(S_0)$
16	639.10		573.60		$\nu_{16}(S_1) = -0.92\nu_{15}(S_0)$
17	674.33	674	583.79		$\nu_{17}(S_1) = -0.83\nu_{16}(S_0)$
18	720.35		621.05		$\nu_{18}(S_1) = +0.51\nu_8(S_0) + 0.42\nu_{19}(S_0)$
19	730.11		633.96		$\nu_{19}(S_1) = -0.73\nu_{17}(S_0) - 0.53\nu_{18}(S_0)$
20	749.55		640.22	648	$\nu_{20}(S_1) = -0.53\nu_{17}(S_0) + 0.39\ \nu_{18}(S_0) - 0.40\nu_{19}(S_0)$
21	833.31	834	692.91	680	$\nu_{21}(S_1) = +0.69\nu_{18}(S_0) + 0.62\nu_{19}(S_0)$
22	837.36		712.00		$\nu_{22}(S_1) = -0.71\nu_{20}(S_0) + 0.60\nu_{25}(S_0)$
23	840.68		799.78	789	$\nu_{23}(S_1) = -0.75\nu_{22}(S_0) - 0.54\nu_{23}(S_0)$
24	876.14		816.44	813	$\nu_{24}(S_1) = +0.51\nu_{23}(S_0) - 0.67\nu_{23}(S_0)$
25	902.84		863.64		$\nu_{25}(S_1) = -0.77\nu_{28}(S_0) - 0.40\nu_{24}(S_0)$
26	905.43	909	864.11		$\nu_{26}(S_1) = +0.83\nu_{24}(S_0)$
27	928.98		875.97		$\nu_{27}(S_1) = -0.86\nu_{26}(S_0)$
28	931.78		903.00	928	$\nu_{28}(S_1) = +0.92\nu_{27}(S_0)$
29	979.29		969.15		$\nu_{29}(S_1) = +0.98\nu_{29}(S_0)$
30	1000.35		979.67		$\nu_{30}(S_1) = +0.86\nu_{30}(S_0)$
31	1025.31	1025	990.31		$\nu_{31}(S_1) = +0.76\nu_{31}(S_0)$
32	1091.20		1013.05		$\nu_{32}(S_1) = -0.76\nu_{34}(S_0)$
33	1097.67		1067.20		$\nu_{33}(S_1) = -0.92\nu_{33}(S_0)$
34	1124.20		1086.05		$\nu_{34}(S_1) = +0.93\nu_{32}(S_0)$
35	1157.63		1112.36		$\nu_{35}(S_1) = -0.56\nu_{40}(S_0) - 0.47\nu_{34}(S_0)$
36	1160.19	1167	1127.99		$\nu_{36}(S_1) = -0.77\nu_{35}(S_0) - 0.54\nu_{36}(S_0)$
37	1176.39		1134.53		$\nu_{37}(S_1) = -0.53\nu_{36}(S_0) - 0.48\nu_{35}(S_0)$
38	1181.18		1169.21		$\nu_{38}(S_1) = +0.67\nu_{37}(S_0) - 0.45\nu_{39}(S_0)$
39	1218.18	1211	1180.37		$\nu_{39}(S_1) = -0.58\nu_{38}(S_0) + 0.50\nu_{37}(S_0)$
40	1252.64	1250	1189.89		$\nu_{40}(S_1) = +0.63\nu_{38}(S_0) + 0.48\nu_{39}(S_0)$
41	1264.30		1243.10		$\nu_{41}(S_1) = +0.95\nu_{41}(S_0)$
42	1279.18	1298	1266.30		$\nu_{42}(S_1) = +0.89\nu_{42}(S_0)$
43	1312.66	1319	1299.68		$\nu_{43}\ (S_1) = +0.55\nu_{44}(S_0) + \ 0.53\nu_{43}(S_0)$
44	1331.32		1302.93		$\nu_{44}(S_1) = -0.50\nu_{44}(S_0) + 0.73\nu_{43}(S_0)$
45	1359.89		1338.56		$\nu_{45}(S_1) = +0.76\nu_{46}(S_0)$
46	1367.55		1355.74		$\nu_{46}(S_1) = -0.95\nu_{45}(S_0)$
47	1373.17		1366.91		$\nu_{47}(S_1) = +0.85\nu_{46}(S_0)$
48	1391.77		1373.22		$\nu_{48}(S_1) = -0.42\nu_{55}(S_0) + 0.35\nu_{49}\ (S_0) - 0.34\nu_{59}(S_0)$
49	1439.08		1378.37		$\nu_{49}(S_1) = -0.56\nu_{48}(S_0) + 0.\ 47\nu_{47}(S_0)$
50	1467.34		1400.97		$\nu_{50}(S_1) = \ +0.53\nu_{55}(S_0) + 0.45\nu_{56}(S_0)$
51	1481.38		1432.01		$\nu_{51}(S_1) = +0.55\nu_{51}(S_0) - 0.\ 46\nu_{57}(S_0)$
52	1488.94	1488	1458.97		$\nu_{52}(S_1) = -0.64\nu_{53}(S_0) - 0.\ 40\nu_{52}(S_0)$
53	1492.64		1468.29		$\nu_{53}(S_1) = -0.50\nu_{49}(S_0) - 0.\ 47\nu_{48}(S_0) - 0.40\nu_{50}(S_0)$
54	1500.40		1470.28		$\nu_{54}(S_1) = +0.46\nu_{50}(S_0) - 0.\ 46\nu_{51}(S_0)$
55	1505.52		1490.21		$\nu_{55}(S_1) = +0.49\nu_{49}(S_0) - \ 0.48\nu_{52}(S_0)$
56	1513.74		1495.55		$\nu_{56}(S_1) = -0.61\nu_{52}(S_0) + 0.43\ \nu_{55}(S_0)$
57	1596.95	1596	1496.13		$\nu_{57}(S_1) = -0.65\nu_{54}\ (S_0) + \ 0.40\nu_{51}(S_0)$
58	1609.24		1579.27		$\nu_{58}(S_1) = -0.51\nu_{58}(S_0) - \ 0.50\nu_{56}(S_0) + 0.42\nu_{57}(S_0)$
59	1652.01	1647	1614.03		$\nu_{59}(S_1) = +0.50\nu_{57}\ (S_0) - 0.46\nu_{58}(S_0) + 0.44\nu_{59}(S_0)$
60	3035.24	2788	2989.30		$\nu_{60}\ (S_1) = -0.93\nu_{61}(S_0)$
61	3036.95		3018.42		$\nu_{61}(S_1) = +0.97\nu_{60}(S_0)$
62	3052.09		3056.69		$\nu_{62}(S_1) = +0.99\nu_{62}(S_0)$
63	3057.84		3062.57		$\nu_{63}(S_1) = +0.98\nu_{63}(S_0)$
64	3085.21	2856	3082.93		$\nu_{64}(S_1) = +0.95\nu_{64}(S_0)$
65	3087.20		3096.91		$\nu_{65}(S_1) = +0.98\nu_{65}(S_0)$
66	3112.95		3122.00		$\nu_{66}(S_1) = +0.99\nu_{66}(S_0)$
67	3117.38	2900	3124.37		$\nu_{67}(S_1) = -0.99\nu_{67}(S_0)$
68	3189.94	2945	3178.33		$\nu_{68}(S_1) = -0.79\nu_{68}(S_0) - 0.61\nu_{70}(S_0)$
69	3195.95		3198.42		$\nu_{69}(S_1) = -0.74\nu_{71}(S_0) - 0.\ 67\nu_{69}(S_0)$
70	3208.53	3030	3220.42		$\nu_{70}(S_1) = -0.63\nu_{70}(S_0) + 0.\ 53\nu_{68}(S_0)$
71	3221.09	3067	3227.45		$\nu_{71}(S_1) = -0.63\nu_{69}(S_0) + 0.52\nu_{71}(S_0)$
72	3656.18	3498	3582.15		$\nu_{72}(S_1) = +1.00\nu_{72}(S_0)$

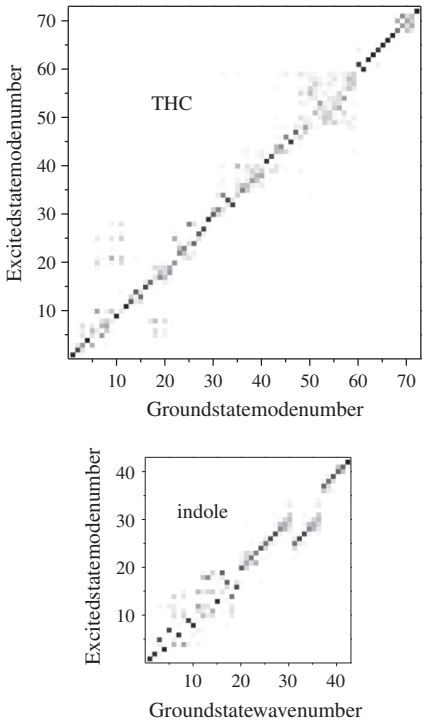

Fig. 2. 72 × 72 Dushinsky matrix of THC (top) and 42 × 42 Dushinsky matrix of indole (bottom), calculated using the numerically determined Hessian at the CC2/cc-pVTZ optimized structures.

From the CC2/cc-pVTZ Hessian for both the ground and L_a excited state, we calculated the Hougen–Watson axis-reorientation matrix, and from this we extracted the three angles ϕ_T, θ_T, and χ_T of reorientation. The results for the general axis reorientation angles are $\theta_T = 0.2°$, $\phi_T = 5.4°$, and $\chi_T = 5.0°$.

Experimental axis reorientation angles, rotational constants, electronic origin frequencies and transition dipole moment angles are compared with the theoretical values for the twist and planar form of THC in Table 3. Clearly, the best agreement between the experimental molecular parameters and the theoretical ones are obtained for the twist conformer. Rotational constants in both electronic states agree closely with those of the twist form and consequently also the inertial defect, which is a measure for the non-planarity of the molecule. The non-zero inertial defect of $-12.2\ \mu A^2$ for the planar (C_s) THC can be traced back to the eight out-of-plane hydrogen atoms of the bridge between C2 and C3, the rest of the molecule being planar. The calculated inertial defect of the twist form is $-21.5\ \mu A^2$, close to the experimental value of $-21.78\ \mu A^2$. The inertial defect hardly changes upon electronic excitation, showing that very small bond lengths and bond angle changes occur in the saturated ring. This is quite different from the case of benzodioxane, which also has a twist conformation in the six-ring. In benzodioxane, the structure of the six-ring was found to be considerably less planar in the excited state as a consequence of the anomeric effect [43].

The geometry change upon electronic excitation to the L_a state of the twist conformer is in much closer agreement, than for the L_b state. One has to keep in mind, that the calculated structure, which is the basis for the rotational constants for the excited state quoted for the L_b state in Table 3 is no stable minimum at the potential energy surface of the S_1 and the S_2 state. The adiabatic excitation energy is also in good agreement with the L_a excitation. The experimentally determined angle of transition dipole moment with the inertial *a*-axis θ is ±16°, the value for the planar axis reorientation angle θ_T is ±0.52°, thus both angles have the same relative sign. The out-of-plane reorientation angles ϕ_T and χ_T have only very small influences on the rovibronic intensities of the spectrum and could not be fit.

The two possible orientations of the TDM angle θ ($-16°$ (I) and +16° (II)) are shown in Fig. 4. They cannot be distinguished from the fit to the intensities alone, since both have the same projection on the inertial *a*-axis. Nevertheless, the absolute determination of the orientation is possible aided by the additional information form the axis reorientation angle θ_T.From the fit we know, that θ and θ_T must have the same sign. From the *ab initio* calculated geometries in the ground and excited state we have determined the angle θ_T to be negative. Thus the absolute orientation of the TDM in THC is like I in Fig. 4a, which in indole is the L_a state. Fig. 4b shows the DFT/MRCI calculated transition dipole moment orientations for the L_a and the L_b state at the respective geometries. While the L_a TDM has nearly the same orientation independent of the reference geometry (S_0 geometry: $-47°$, S_1 geometry: $-48°$, S_2

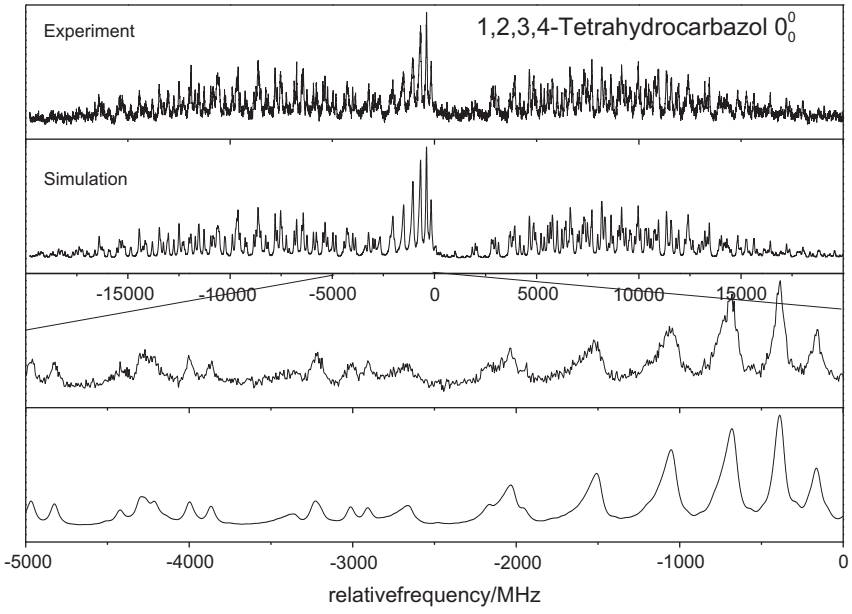

Fig. 3. Rotationally resolved electronic spectrum of the origin band of THC along with the simulation using the best fit parameters.

Table 3
CC2/cc-pVTZ calculated relative energies, rotational constants (A, B, C), their changes upon electronic excitation (ΔA, ΔB, ΔC), inertial defects (ΔI), DFT/MRCI calculated center frequency of absorption (ν_0), and orientations of the transition moment (θ and ϕ) of the planar and the twist conformers of THC. Doubly primed quantities refer to the ground state, primed quantities to the excited singlet states.

	Planar	Twist		Exp.
	$L_a \leftarrow S_0$	$L_a \leftarrow S_0$	$L_b \leftarrow S_0$[a]	
E_{rel} (cm^{-1})	4259	0		–
A'' (MHz)	2019	2050		2043.4(17)
B'' (MHz)	555	563		560.46(5)
C'' (MHz)	440	450		448.36(4)
$\Delta I''$ (μA^2)	−12.2	−21.5		−21.78(5)
ν_0 (cm^{-1})	36669	34976	35889	34786.63(2)
θ (°)	−8	−47	+42	±16(5)
θ_T (°)	−0.05	−0.67	−0.77	±0.52(10)
$\Delta I'$ (μA^2)	−12.2	−21.1	−21.4	−21.6(5)
ΔA (MHz)	−14	−24	−12	−41.21(3)
ΔB (MHz)	−9	−3	−10	−0.84(1)
ΔC (MHz)	−6	−3	−7	−2.62(1)

[a] Keep in mind, that the L_b state is no stable minimum nor on the S_1 neither on the S_2 surface. For details see text.

geometry: −50°), the L_b TDM depends extremely on the chosen reference geometry (S0 geometry: +1°, S_1 geometry: +58°, S_2 geometry: +42°).

4. Conclusions

The structure of THC has been determined from a combination of rotationally resolved electronic spectroscopy and *ab initio* theory to be planar in the indole chromophore and twisted in the saturated six-ring in both the electronic ground and first excited singlet state. From the measured orientation of the transition dipole moment, the lowest electronically excited state has been determined to be of L_a character, what has been confirmed by *ab initio* calculations. Both CC2 and DFT/MRCI, consistently predict the L_a to be adiabatically the lowest state. The calculated structural changes (measured by the changes of the rotational constants upon electronic excitation) and the zero-point energy corrected origin frequency are also in good agreement with the supposition of a L_a state being responsible for the absorption features of THC.

The calculated vertical transition to the excited state in the Franck-Condon region has clear L_b character. No stable minimum for this configuration has been found at CC2 level of theory, instead the geometry rapidly develops into that of the L_a state. This result implies, that the transition from the L_b potential to the L_a is virtually barrierless as sketched in the right part of Fig. 5. Both L_a and L_b states are strongly mixed above the crossing, whose upper limit is about 1000 cm^1 above the L_a minimum. Therefore, we prefer to label the excited states by their energetic ordering as S_1 and S_2 states, respectively. In the adiabatic description, electronically L_a- and L_b-like minima are than found at different geometries on the S_1 surface, while in the diabatic picture, a crossing exists, very close to the onset of the L_b state. The upper limit for the $L_a - L_b$ energy difference agrees roughly with the intensity break-off of the vibronic spectrum, giving further evidence for the above model. Diabatically spoken, the minimum of the L_b state is so close to the intersection between the L_a and L_b state, that practically every nuclear motion acts as "tuning mode" for the crossing. Thus, even the zero-point-motion promotes the passage from the L_b to the L_a state. On the other hand, the closeness of the L_a and L_b minima can mix L_b character into the electronic L_a wavefunction at the origin through Herzberg–Teller-like vibronic coupling using the zero-point-motions. This might explain the numerical deviations of the TDM orientation between the DFT/MRCI calculations and the experimental values, which are larger than for comparable systems. An explanation, why the L_a origin of the isolated THC lies under the onset of the L_b state might be given from consideration of the electronic properties of the substituents. Methyl groups exert a positive inductive +I-effect, shifting electron density into the chromophore. In indole, the L_a origin lies about 1400 cm^1 above the L_b origin [15]. This gap is reduced to roughly 500 cm^1 for the monosubstituted 3-methylindole [44] and to below 400 cm^1 for the disubstituted 2,3-dimethylindole [21]. Thus, the L_a/L_b gap seems to depend on variations of the electron density in the region of the C2 and C3 atoms. In THC, the bridge can be thought as being composed of two ethyl groups, with an inherently larger +I-effect, that might be responsible for switching the energetic order of the L_a and L_b states. Alternatively, the modification of the C2–C3 stretching coordinate, which is also the tuning mode for the L_a/L_b conical intersection by bridging the two positions, might be responsible for the switching of the states. Comparison of the C2–C3 bond length of THC with that of indole shows, that in the electronic ground state, the bond length increases by 0.5 pm. Upon excitation to the L_a state, a large increase of the bond length is found for indole (+6.3 pm) and an even larger for THC (+6.9 pm), while the bond length changes upon excitation to the L_b state are much smaller (+0.6 pm for indole and +1.4 pm for THC). Thus, it might even be, that a strain, which the six-ring exerts on the C2–C3 bond, stabilizes the L_a state more than the L_b. Keep in mind, that the six-ring in THC is in a twist conformation, whose energy in cyclohexane is by 21 kJ/mole higher than of the unstrained chair

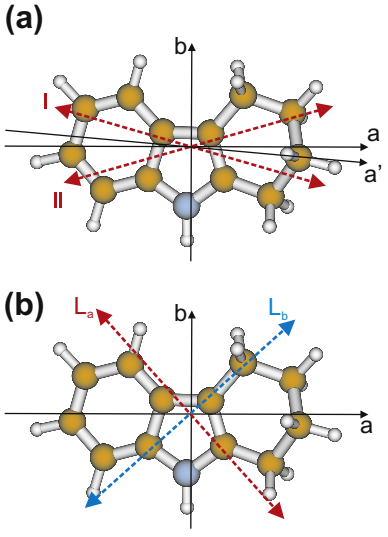

Fig. 4. (a) Possible orientation of the TDM from the experiment. The axis reorientation angle ($a \rightarrow a'$) has been exaggerated by a factor 10 for sake of clarity. (b) DFT/MRCI calculated transition dipole moment orientations for the L_a (red) and the L_b state (blue).

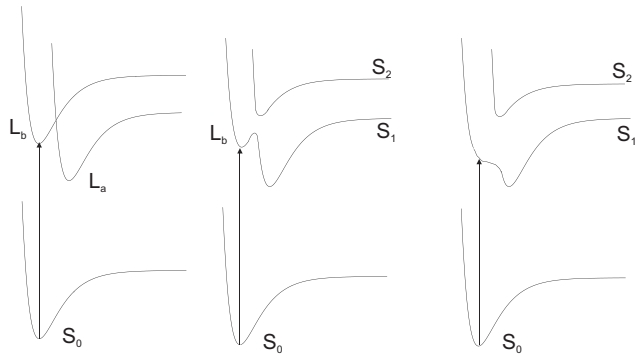

Fig. 5. Excitation scheme of THC in the diabatic (left) and adiabatic (middle) limit. The right part represents a small or absent barriers between the minima on the S_1 state potential energy surface.

conformation. In this case, the low-lying L_a state in 2,3-dimethylindole would be at least partially a consequence of the van der Waals strain of the two methyl groups.

A definite answer on the question, which of these mechanisms is responsible for the switching of states in THC, can be expected from an investigation of the mixed 2-methyl-3-ethyl-indole, 3-methyl-2-ethyl-indole, and 2,3-diethylindole, which are planned in our group.

Acknowledgments

This work was supported by the Deutsche Forschungsgemeinschaft in the framework of the NWO-DFG bilateral program Grant No. SCHM1043/10 (Germany) and DN 72-248 (The Netherlands).The authors would like to thank the National Computer Facilities of the Netherlands Organization of Scientific Research (NWO) for a grant on the Dutch supercomputing facility SARA. Granted computing time at Universitatsrechenzentrum Koln is gratefully acknowledged.

Appendix A. Supplementary data

Supplementary data associated with this article can be found, in the online version, at doi:10.1016/j.molstruc.2011.01.029.

References

[1] M.R. Eftink, Methods Biochem. Anal. 35 (1991) 127.
[2] J.T. Vivian, P.R. Callis, Biophys. J. 80 (2001) 2093.
[3] J. Zuclich, J.U. von Schütz, A.H. Maki, J. Am. Chem. Soc. 96 (1974) 710.
[4] B.J. Fender, K.W. Short, D.K. Hahn, P.R. Callis, Int. J. Quantum Chem. 72 (1999) 347.
[5] J.W. Hager, S.C. Wallace, J. Phys. Chem. 87 (1983) 2121.
[6] J.W. Hager, S.C. Wallace, J. Phys. Chem. 88 (1984) 5513.
[7] M.J. Tubergen, D.H. Levy, J. Phys. Chem. 95 (1991) 2175.
[8] J.R. Carney, F.C. Hagemeister, T.S. Zwier, J. Chem. Phys. 108 (1998) 3379.
[9] K. W Short, P.R. Callis, J. Chem. Phys. 108 (1998) 10189.
[10] C. Kang, T.M. Korter, D.W. Pratt, J. Chem. Phys. 122 (2005) 174301.
[11] D.M. Sammeth, S. Yan, L.H. Spangler, P.R. Callis, J. Phys. Chem. 94 (1990) 7340.
[12] M.R. Eftink, L.A. Selvidge, P.R. Callis, A.A. Rehms, J. Phys. Chem. 94 (1990) 3469.
[13] B. Albinsson, B. Nordén, J. Phys. Chem. 96 (1992) 6204.
[14] T.L.O. Barstis, L.I. Grace, T.M. Dunn, D.L. Lubman, J. Phys. Chem. 97 (1993) 5820.
[15] B.J. Fender, D.M. Sammeth, P.R. Callis, Chem. Phys. Lett. 239 (1995) 31.
[16] G. Berden, W.L. Meerts, E. Jalviste, J. Chem. Phys. 103 (1995) 9596.
[17] A.L. Sobolewski, W. Domcke, Chem. Phys. Lett. 315 (1999) 293.
[18] C. Brand, J. Küpper, D.W. Pratt, W.L. Meerts, D. Krügler, J. Tatchen, M. Schmitt, Phys. Chem. Chem. Phys. 12 (2010) 4968.
[19] J. Küpper, D.W. Pratt, W.L. Meerts, C. Brand, J. Tatchen, M. Schmitt, Phys. Chem. Chem. Phys. 12 (2010) 4980.
[20] J.R. Platt, J. Chem. Phys. 17 (1949) 484.
[21] K.W. Short, P.R. Callis, Chem. Phys. 283 (2002) 269.
[22] B. Fender, P.R. Callis, Chem. Phys. Lett. 262 (1996) 343.
[23] A.A. Rehms, P.R. Callis, Chem. Phys. Lett. 140 (1987) 83.
[24] C.K. Teh, A. Gharavi, M. Sulkes, Chem. Phys. Lett. 156 (1990) 460.
[25] P.R. Callis, J. Chem. Phys. 95 (1991) 4230.
[26] J.W. Hager, D.R. Demmer, S.C. Wallace, J. Phys. Chem. 91 (1984) 5513.
[27] D.R. Demmer, G.W. Leach, E.A. Outhouse, J.W. Hager, S.C. Wallace, J. Phys. Chem. 94 (1990) 582.
[28] M. Schmitt, J. Kupper, D. Spangenberg, A. Westphal, Chem. Phys. 254 (2000) 349.
[29] S. Gerstenkorn, P. Luc, Atlas du spectre d'absorption de la molécule d'iode, CNRS, Paris, 1982.
[30] R. Ahlrichs, M. Bär, M. Häser, H. Horn, C. Kölmel, Chem. Phys. Lett. 162 (1989) 165.
[31] J.T.H. Dunning, J. Chem. Phys. 90 (1989) 1007.
[32] C. Hättig, F. Weigend, J. Chem. Phys. 113 (2000) 5154.
[33] C. Hättig, A. Köhn, J. Chem. Phys. 117 (2002) 6939.
[34] C. Hättig, J. Chem. Phys. 118 (2002) 7751.
[35] S. Grimme, M. Waletzke, J. Chem. Phys. 111 (1999) 5645.
[36] A.D. Becke, J. Chem. Phys. 98 (1993) 1372.
[37] C. Lee, W. Yang, R. Parr, Phys. Rev. B 37 (1988) 785.
[38] N. Hansen, A. Ostermeier, Evolut. Comput. 9 (2001) 159.
[39] C. Brand, O. Oeltermann, D.W. Pratt, R. Weinkauf, W.L. Meerts, W. van der Zande, K. Kleinermanns, M. Schmitt, J. Chem. Phys. 133 (2010) 024303.
[40] K. Feng, Dispergierte Fluoreszenzspektroskopie an Heteroaromaten und deren Cluster in der Gasphase, PhD Thesis, Heinrich-Heine-Universität, Düsseldorf, 2009.
[41] J.T. Hougen, J.K.G. Watson, Can. J. Phys. 43 (1965) 298.
[42] A. Held, B.B. Champagne, D.W. Pratt, J. Chem. Phys. 95 (1991) 8732.
[43] T.B.C. Vu, C. Brand, W.L. Meerts, M. Schmitt, ChemPhysChem. (2011), doi:10.1002/cphc.201000576.
[44] D.M. Sammeth, S.S. Siewert, L.H. Spangler, P.R. Callis, Chem. Phys. Lett. 193 (1992) 32.